



Minerals from Macedonia. XX. Geological Setting, Lithologies, and Identification of the Minerals from Ržanovo Fe-Ni Deposit

BLAŽO BOEV¹, GLIGOR JOVANOVSKI^{2,3,*} & PETRE MAKRESKI²

¹ Faculty of Mining, Geology and Polytechnic, Goce Delčev University, Goce Delčev 89,
MK-2000 Štip, Republic of Macedonia
(E-mail: blazo.boev@ugd.edu.mk)

² Institute of Chemistry, Faculty of Science, SS. Cyril and Methodius University,
P.O. Box 162, MK-1001 Skopje, Republic of Macedonia

³ Macedonian Academy of Sciences and Arts, Bul. Krste Misirkov 2, P.O. Box 428,
1000 Skopje, Republic of Macedonia

Received 07 August 2007; revised typescript received 24 March 2008; accepted 31 October 2008

Abstract: The Ržanovo deposit lies within the western ophiolite belt of the Vardar zone. Its main geological units are discussed in terms of their mineralogy, petrology and petrological evolution. Minerals observed include: magnetite, hematite, clinocllore, talc, sepiolite, magnesioriebeckite, lizardite, dolomite, phlogopite, stilpnomelane, quartz, albite, pyrite, maghemite, pyrrhotine, digenite and millerite. Some minerals had non-distinct morphologies and ambiguous characteristics, preventing identification on the basis of physical properties alone. Thus, some of the minerals (magnetite, hematite, talc, dolomite, olivine, calcite, aragonite and brucite) as well as some serpentine minerals (antigorite and chrysotile) were identified by vibrational spectroscopy. Difficulties in identification by IR spectroscopy and Raman were considered to be the result of contamination (i.e., inclusions of other minerals in the analyzed crystals).

Key Words: Ržanovo, mineral deposit, geology, mineralogy, vibrational spectroscopy

Makedonya XX'den Mineraller: Jeolojik Konum, Litolojiler ve Ržanovo Fe-Ni Cevherinden Mineral Tanımlamaları

Özet: Ržanovo cevheri Vardar zonu'nun batı ofiyolit kuşağında yer almaktadır. Cevher zonunun ana jeolojik özellikleri, mineralojisi, petrolojisi ve petrolojik evrimi dikkate alınarak tartışılacaktır. Magnetit, hematit, klinoklor, talk, sepiyolit, magnesioriebekit, lizardit, dolomit, fiogopit, stilpnomelan, kuvars, albit, pirit, maghemit, firohottin, digenit ve millerit gibi mineraller cevher zonunda gözlemlenmiştir. Belirgin olmayan morfolojileri ve özellikleri bazı minerallerin sadece fiziksel özellikleri kullanılarak tanımlanmasını zorlaştırmaktadır. Bunun için, magnetit, hematit, talk, dolomit, olivin, kalsit, aragonit ve brusite ile bazı serpentin mineralleri (antigorit ve krizotil) titreşimli spektroskopisi yöntemi ile tanımlanmışlardır. Analiz edilen mineral içinde diğer minerallerin inklüzyonlarının varlığı IR spektroskopisi ve Raman yöntemleri ile minerallerin tanımlanmasını zorlaştırmıştır.

Anahtar Sözcükler: Ržanovo, mineral cevheri, jeoloji, mineraloji, titreşimli spektroskopisi

Introduction

Deposits of nickel and nickeliferous iron silicate in the Vardar zone are situated in a relatively narrow ophiolite belt that stretches from Fruška Gora in the

north to Euboea in the south, thence continuing to Anatolia in Turkey. The central part of this zone is shown in Figure 1. Spatially and in some part genetically, primary deposits are related to the

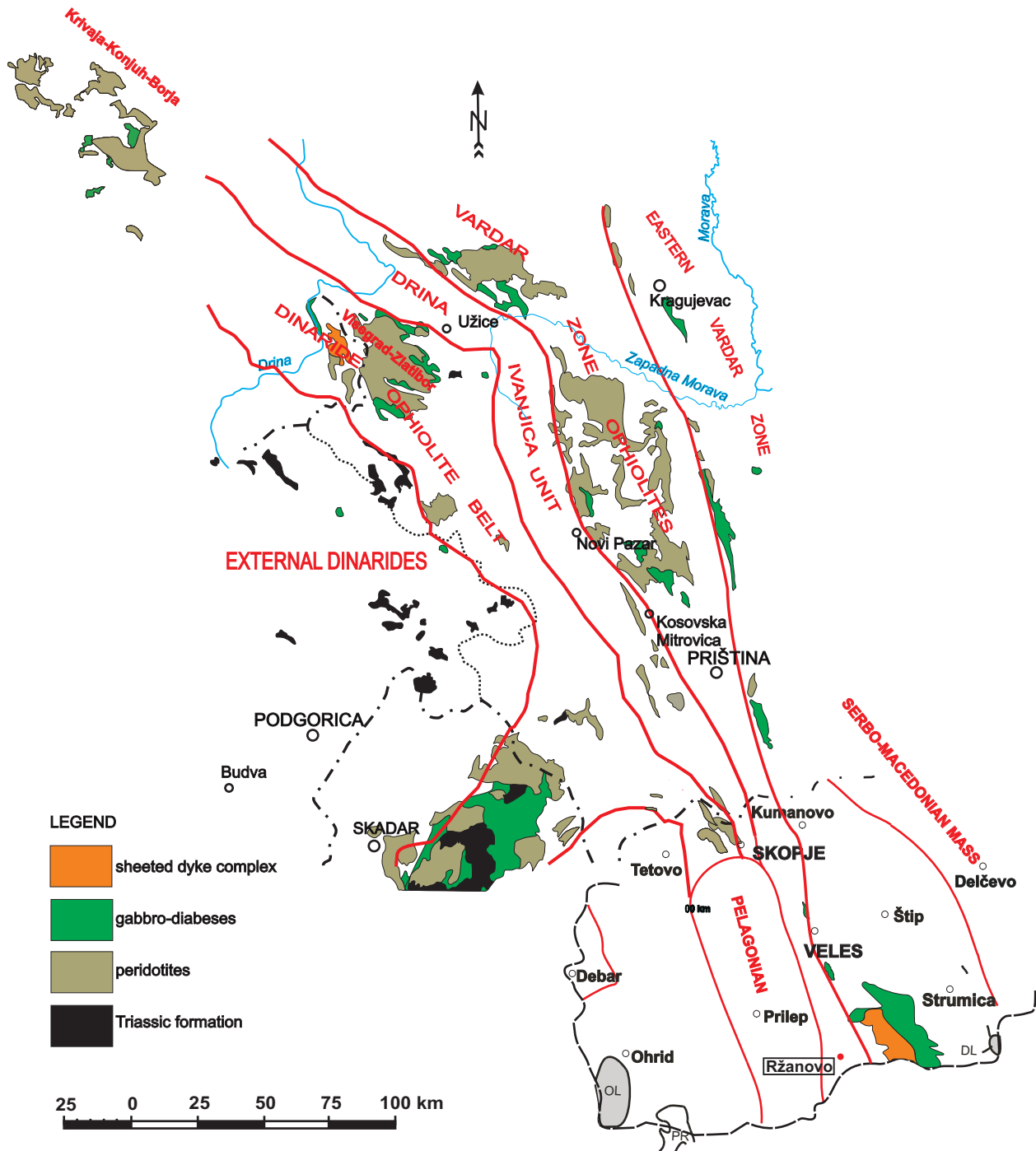


Figure 1. Distribution pattern of the ophiolites in the Vardar zone.

peridotite complexes of the Jurassic ophiolite formations, or more precisely, to the weathering crusts developed on the peridotites/serpentinites in wet and warm climates conditions as a result of surface processes.

Most of the ancient weathering crust was eroded during later processes, particularly in conditions of dissected palaeorelief. Residual deposits of Ni-silicates remained in place, where they were either covered by younger sediments that protected them

from further erosion or were redeposited in surrounding basins or nearby karstified vugs/troughs.

Although the nickeliferous mineralization in weathering crusts in the Vardar zone was known before 1941, excavation of ores only began after 1970. Two metallurgical plants were built: The FENI in the town of Kavadarci (Boev & Jankovic 1996), and Glogovac Plant near the town of Priština. The occurrences of nickel and nickeliferous iron in the western ophiolite belt (in Albania and Greece) were put into production much earlier than those in the Vardar zone.

The Ržanovo Fe-Ni ore deposit, part of the Ržanovo-Studena Voda ore series, crops out in the southern part of Republic of Macedonia near the Greek border. The deposit is situated within the west ophiolitic belt of the Vardar zone, which is a major geotectonic unit in the geological structure of Republic of Macedonia.

The first investigation of the Ržanovo nickel ores were presented by Ivanov (1959), and preliminary studies of the ore mineralogy were reported by Grafenauer & Strmole (1966) and Maksimović & Panto (1981).

Experimental

All the studied minerals were collected from Ržanovo. Single crystals of the investigated minerals were carefully selected under a microscope from the ore samples and then powdered.

Chemical compositions of the individual minerals were analyzed using the electron microprobe (EMP) Cameca Microprobe Analyzer. The accelerating voltage was set to 15 kV and the current power was adjusted to 15 mA. Natural minerals were used as standards and counting time was 6 seconds. The presented mineral analyses represent average values obtained from three different points.

A Perkin-Elmer FTIR system 2000 interferometer was employed to record the spectra using the KBr pellet method. The pellet was prepared by distributing 1 mg of the powdered sample into 250 mg KBr (for IR spectroscopy, Merck) and applying a

pressure of 10 t/cm². The resolution of the instrument was 4 cm⁻¹ and for each IR spectrum 16 scans (accumulations) were collected. For acquisition of Spectra GRAMS ANALYST 2000 software was used.

The Raman spectra were recorded using a computerized Dilor Z24 triple dispersive monochromator with Coherent Innova 400 argon ion laser operating at 514.5 nm. Laser power of 50 or 100 mW was applied depending on mineral sensitivity whereas the slit was 500 microns. To reduce the heating of the sample, the incident laser beam was modified in line shape focus. Measurements were carried out at room temperature and spectral data were analyzed with GRAMS/32 package.

The Kožuf Ore District

The Kožuf ore district is situated on Kožuf Mountain near the Macedonian-Greek border. The Ržanovo deposit, one of the largest in the Vardar zone, is situated close to the contact between the Vardar zone and the Pelagonian massif in a tectonically active area.

General Geological Setting of the Ržanovo Zone

The investigated area is a part of the western ophiolite belt of the Vardar zone and essentially consists of several lithostratigraphic units with distinct mineralogy, petrology and evolution. The main units which comprise the geological setting are shown in the geological map (Figure 2), and include: (i) Tertiary volcanic rocks and pyroclastics, (ii) limestones of Albian–Cenomanian age, (iii) lateritic Fe-Ni ores of the Cretaceous age, (iv) ultrabasic complexes (serpentinites) with gabbro-pegmatites and rodingites, (v) schistose series of Palaeozoic (?) age (phillites, argillites and quartzites).

Several large dislocations pass through the host ultrabasic masses. The Ržanovo overthrust zone is present as several parallel thrusts in which ultrabasic rocks (dunite and harzburgite), schists and marble alternate. The ore series in the thrusts is dismembered and disappears in some places.

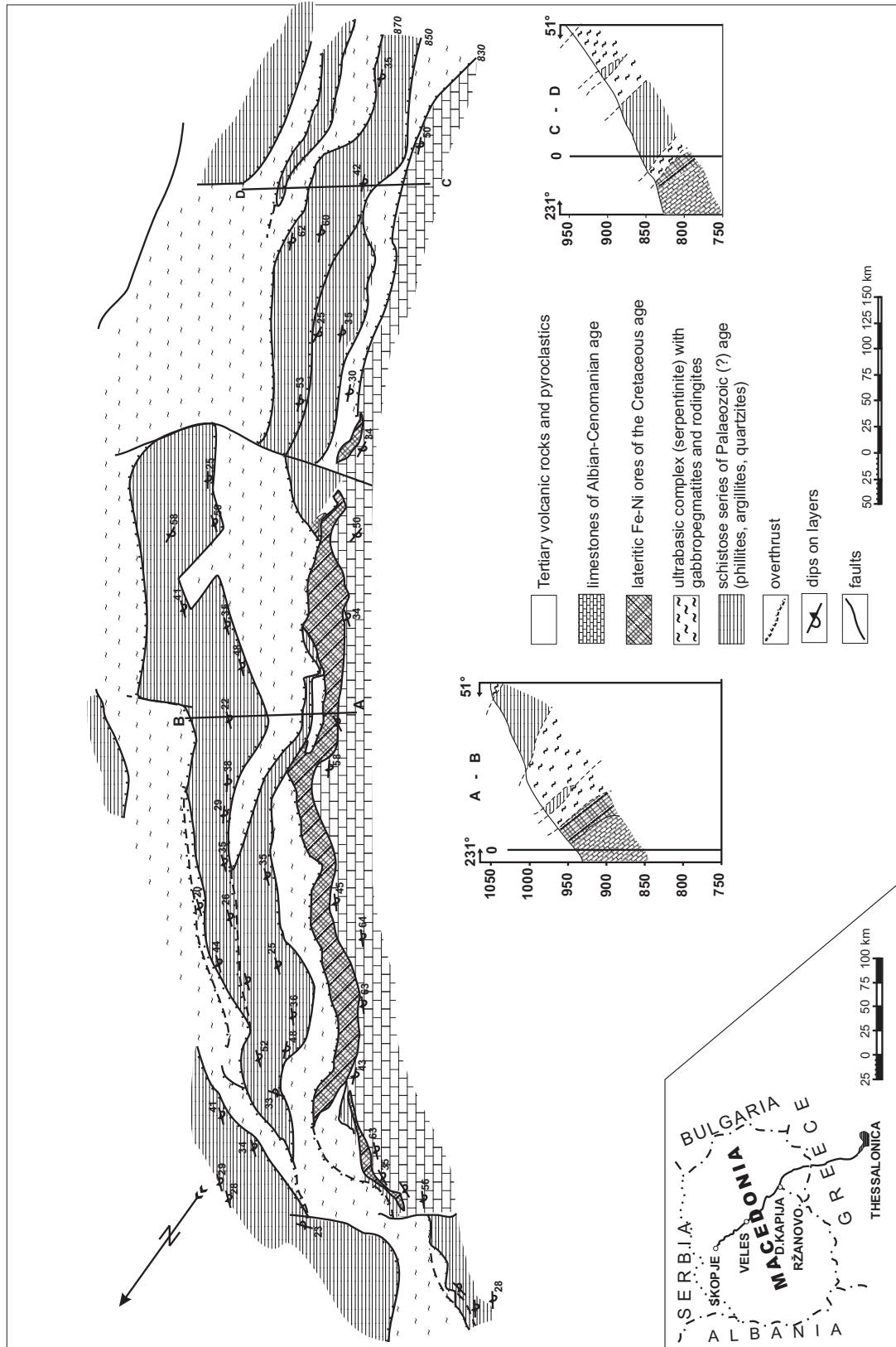


Figure 2. Geological map of the Ržanovo zone.

The Ržanovo ore zone can be traced for more than 4 km with a thickness varying from 1 to 40 m. The ore zone is inhomogeneous in texture and consists of several lithological and ore varieties (Stojanov & Boev 1985). The rocks most affected by weathering processes are ultrabasic rocks.

Main Characteristics of the Schistose Series

Microscopic examinations determined that schists consist of quartz, sericite (illite), chlorite, albite and talc. The mineral composition indicates that primary clays were transformed into schists under conditions of greenschist facies metamorphism.

Metasandstone lenses occasionally occur in the series together with quartzite. They consist of quartz grains, rare microcline or plagioclase and very rare tourmaline. The slightly rounded to angular grains are often distorted indicating that structural deformation accompanied metamorphism.

The mainly siliceous matrix is completely recrystallized and contains small amounts of calcite, indicating that the protolith was an arkose originally with a quartz matrix or a poor clayey siliceous matrix.

Ultrabasic Complexes

The *gabbro-peridotite* complex in the Ržanovo zone is located in the western part of the Vardar zone (Karamata 2006). It consists predominantly of peridotites, gabbro-pegmatites and rodingites.

Dunites and harzburgites are the main members of the Alpine-type ultramafic rocks in the Ržanovo zone. Harzburgites are distinguished by the presence of enstatite grains 1 cm across. Based on field relationships and microscopic studies the term dunite and harzburgite are conditionally used as they are heavily serpentinized. Serpentinized harzburgites generally occur as compact blocks and contain pyroxene crystals up to 1 cm in size which can be clearly seen.

Serpentine occurs with net-like texture originating from pyroxene. Individual flakes and fibres of serpentine minerals are parallel to one another and possess primary mineral cleavage. In some places pyroxenes are not completely altered to serpentine minerals but are affected by bastitization.

Microscope studies indicate that in some cases serpentine replaces olivine. It is net-like and individual flakes or fibres of serpentine minerals are arranged along irregular cracks within the primary olivine grains (the first generation serpentine) and as ring radial aggregates replacing individual parts of olivine grains (the second generation serpentine). Some magnetite develops as magnetite powder during the serpentinization process.

Gabbro-pegmatite-rodingites in the Ržanovo area are elongated and cross-cut the blocks of serpentinites. They are small and can easily be recognized on the field. Fresh gabbro-pegmatites unaffected by rodingitization processes are rare and coarse-grained, with monoclinic pyroxene grains in some places up to 30 cm across. Microscope investigations show that they mainly consist of basic plagioclase and monoclinic pyroxene. Pyroxenes are chloritized and prehnitized, whereas plagioclase is sometimes replaced by prehnite, clearly indicating the beginning of rodingitization.

Rodingites are mainly located in the marginal parts of the serpentinite mass as elongate blocks of variable thickness. They are formed from gabbros and gabbro-pegmatites during a postmagmatic phase of replacement due to calcium metasomatism. They essentially consist of garnet (hydrogrossular hibschite), monoclinic pyroxene (diopside, xenomorphic grains), prehnite and vesuvianite. Garnets are mainly replaced by plagioclase. Pyroxenes are affected by prehnitization, uralitization and chloritization (Boev *et al.* 1999).

Cretaceous Lateritic Fe-Ni Ores

The Ržanovo ore zone can be traced for more than 4 km with a thickness varying from 1 to 40 m. The ore body itself is 1500 metres long and is between 17 and 33 metres thick. Its surface is occasionally disrupted as a result of tectonic movements. The ore body generally trends north-south and dips sub-vertically. The ore layer is texturally inhomogenous.

Limestones of Albian-Cenomanian Age

The weakly metamorphosed Albian-Cenomanian limestones represent the top part of the ore-bearing series in the Ržanovo area. Locally, they are

tectonically inverted. Where tectonic deformation is intense the carbonate base comprises completely recrystallized calcite (Ivanov *et al.* 1987).

Tertiary Volcanic Rocks and Pyroclastics

This series in the Ržanovo area is a part of the large Kožuf Mountain volcanic complex. The volcanic series, comprising Pliocene calc-alkaline rocks, consists of latites, quartz latites, trachytes, andesites as well as a huge amount of pyroclastic tuffs and breccias.

The Ržanovo Deposit

The deposit was discovered by Ivanov (1959), although some data were reported earlier. Nickeliferous iron ore mineralization is located along the contact between the Jurassic serpentinites and schists in the footwall and the Cretaceous limestones in the hanging wall. The ore layer was explored to a depth of about 500 m with an average thickness of 30 m. It appears as a continuous sub-vertical body. Strong post-emplacement tectonic movements in part of the Ržanovo deposit have caused overthrusting (Figure 2), although the ore layer retains a homogenous appearance. However, based on its geochemical-mineralogical features the ore body is actually heterogeneous and comprises several lithological members with their own mineralogy and chemistry. Based on available knowledge of the Ržanovo ore body the following textural ore/rock types are distinguished: (i) massive magnetite ore, (ii) schistose magnetite ore, (iii) oolitic magnetite ore, (iv) schistose hematite ore, (v) compact hematite ore, (vi) riebeckite schists, (vii) stilpnomelane schists, (viii) dolomite-talc schists, (ix) talc schists, and (x) serpentinites.

Massive Magnetite Ore

This member is found close to the hanging wall or the top part of the ore layer. It consists of massive compact magnetite ore in which magnetite dominates. Besides magnetite, other minerals present (Table 1) include hematite, clinocllore, talc, sepiolite, dolomite and amphibole.

The chemical composition of the Ni-Fe ores in the Ržanovo deposit is shown in Table 2 and analyses of trace elements in individual lithological types of ore are given in Table 3.

Schistose Magnetitic Ore

This type of ore is characterized by a distinctive relationship between the minerals magnetite, hematite, talc, clinocllore, amphibole and dolomite, resulting in different chemical features. Their ratios are shown in Table 1.

The chemistry shows that this type of ore is relatively rich in nickel (1.0 wt%, Table 2) and sodium (0.84 wt%) indicating the presence of magnesioriebeckite amphibole. Trace element contents in the ore are presented in Table 3, with elements derived from ultramafics dominant such as nickel, cobalt and chromium.

Oolitic-hematitic Ore

This type of ore is very common in the Ržanovo ore deposit. It has a clear oolitic-pisolitic structure. Investigations showed that this type of ore contains: magnetite, hematite, talc, clinocllore and amphibole, with minor sepiolite. Relations of the individual minerals are given in Table 1.

The chemical composition of this type of ore is given in Table 2. The nickel content in the ore averages 1.21 wt% and the sodium content is 0.93 %. This lithological type of ore is very rich in iron because of the abundance of hematite (Table 3).

This type of ore is enriched in trace elements originating from ultramafic rocks. Zirconium is also abundant (275 ppm) coming from more acidic rocks, probably schists.

Schistose Hematitic Ore

This ore lithology is the most abundant in the Ržanovo deposit. Characteristically schistose, its most common minerals are: magnetite, hematite, talc, clinocllore and amphibole with sporadic pyrite. Relative abundances of the minerals are given in Table 1.

Table 1. Quantitative mineralogical compositions of the Fe-Ni ore types in the Ržanovo deposit (in mass %).

	Massive magnetite ore	Schistose magnetite ore	Oolitic magnetite ore	Schistose hematite ore	Compact hematite ore	Riebeckite schists	Stilpnomelane schists	Dolomite-talc chists	Talc schists	Serpentinities
Mt	68	25	11	6	9				15	11
Hm	1	18	56	60	51			18	7	21
Clh	9	20	13	13	8					
Tc	9	16	13	10	15	6	20	24	64	30
Se	9	5	5							
Amf	2	14	2	10	15	53		24		
Do	1	1		1		5	3	26		6
Py							5			
Stl							42			
Mgh							7			
Liz						6	10	6	9	30
Phlo						2				
Ab						10				
Q							11			
Dig						6				
Pyht						9				
Sid										
Total	99	99	100	100	98	97	98	98	95	98

Mt- magnetite, Hm- hematite, Clh- clinocllore, Tc- talc, Se- sepiolite, Amf- amphibole, Do- dolomite, Py- pyrite, Stl- stilpnomelane, Mgh- maghemite, Liz- lizardite, Phlo- phlogopite, Ab- albite, Q- quartz, Dig- digenite, Pyht- pyrrhotite, Sid- siderite.

Table 2. Chemical composition of the Ni-Fe type of ores in the Ržanovo deposit (in mass %).

	Massive magnetite ore	Schistose magnetite ore	Oolitic magnetite ore	Schistose hematite ore	Compact hematite ore	Riebeckite schists	Stilpnomelane schists	Dolomite-talc chists	Talc schists	Serpentinities
Al ₂ O ₃	1.78	3.89	2.92	2.36	2.91	6.60	1.88	1.20	1.05	1.39
CaO	0.98	1.47	2.57	2.30	1.26	1.98	2.90	3.79	1.63	1.37
Cr ₂ O ₃	1.68	2.26	2.26	1.79	3.23	7.00	2.66	0.95	0.36	0.39
T Fe ₂ O ₃	32.91	41.01	58.37	43.97	42.32	16.72	40.05	19.72	11.17	12.35
H ₂ O	0.24	1.22	0.86	0.38	0.48	0.28	1.31	0.14	0.30	0.73
K ₂ O	0.10	0.60	0.10	0.10	0.10	0.22	0.81	0.18	0.18	0.20
LOI	2.65	3.00	2.17	3.24	3.36	0.16	9.08	4.13	5.67	9.68
MgO	18.40	11.37	8.21	13.94	15.31	7.62	8.36	18.88	28.64	31.67
MnO	0.24	0.32	0.35	0.37	0.64	0.73	0.23	0.81	0.26	0.16
Na ₂ O	0.50	0.84	0.93	0.58	0.63	5.07	0.80	0.84	0.59	0.83
NiO	0.90	1.0	1.21	1.08	1.06	2.13	1.10	0.87	0.75	0.37
P ₂ O ₅	0.17	0.53	0.32	0.53	0.31	0.36	0.38	0.34	0.40	0.40
SiO ₂	40.02	32.38	19.84	26.64	28.59	46.33	25.37	48.79	48.77	41.31
SO ₃	0.47	1.50	0.50	0.74	0.50	2.82	3.72	0.32	0.26	0.26
TiO ₂	0.02	0.07	0.03	0.03	0.03	0.28	0.18	0.01	0.01	0.01
Total	101.06	101.46	100.64	98.05	100.73	98.3	98.83	100.97	100.04	101.12

Table 3. The results from the EMS analyses of trace elements in individual lithological types of ore in the Ržanovo deposit (in ppm).

	Massive magnetite ore	Compact hematite ore	Schistose magnetite ore	Oolitic hematite ore	Schistose hematite ore
B	15	18	20	20	20
Ba	64	17	20	18	30
Co	205	148	235	480	150
Cr	> 1%	> 1%	> 1%	> 1%	> 1%
Cu	9	3	9	18	5
Ga	3.5	3	4	7	7
Mn	830	1780	3020	2090	775
Ni	8880	> 1%	8490	> 1%	8725
Pb	22	14	19	62	47
Sc	27	11	20	33	29
Sr	52	85	250	24	105
V	120	66	118	195	163
Zn	355	180	230	185	290
Zr	84	40	110	275	140

Nickel and sodium average 1.08 % and 0.58 %, respectively. Iron content is relatively high and the magnesium content ranges between 12 and 17 % (Table 2).

Massive Hematite Ore

This type of ore is also common in the Ržanovo ore deposit. Texturally massive and hard, it contains the following mineral association: magnetite, hematite, clinocllore, talc, and amphibole. The proportion of minerals is given in Table 1.

Chemical analyses of the ore (Table 2) indicate that it is relatively rich in nickel – 1.06 % NiO. Large sodium contents (0.63 %) indicate the abundance of amphibole in the ore (Table 2) whereas the analyses of trace elements identify high contents of nickel, chromium and cobalt (Table 3).

Riebeckite and Stilpnomelane Schists

This type of ore is less common in the Ržanovo deposit. It can easily be distinguished from other types by both its colour and structure. It can be considered as a typical metamorphic rock. Riebeckite rocks are blue and stilpnomelane are yellowish in colour. Riebeckite schists are mainly composed of riebeckite, talc, lizardite, phlogopite, digenite and pyrrhotite whereas stilpnomelane

schists consist of stilpnomelane, talc, maghemite, lizardite, dolomite, quartz and pyrite. The proportions of individual minerals are given in Table 1.

Chemical analyses (Table 2) indicate that both riebeckite and stilpnomelane schists are rich in nickel. Nickel content in riebeckite schists is over 2 % and in stilpnomelane within 1.1 %.

Dolomite-talc Schists

This lithological type of mineralization is also rarer in the Ržanovo deposit. It differs from other types in its colour. The rocks with large contents of iron minerals have a reddish colour. The mineral composition of this type includes talc, dolomite, hematite, magnetite, amphibole, lizardite and clinocllore. Proportions of individual minerals are given in Table 1.

Chemical analysis (Table 2) indicates that this type of ore contains less nickel than other types (0.87 % NiO). It is characterized by its large content of calcium, sodium and magnesium.

Talc Schists

This lithological type of ore occurs sporadically in the Ržanovo deposit. It can be seen along tectonic

zones and tectonic mirrors. It is greenish in colour and contains small magnetite crystals. It is mostly composed of talc, clinocllore, magnetite, hematite and lizardite. Proportions of individual minerals are given in Table 1.

The chemical composition shown in Table 2 indicates that the ore is rich in magnesium and silica, whereas the iron content is relatively low compared to other ore types. The nickel content is 0.75 %.

Serpentinite

This common member of the Ržanovo deposit, comprising several minerals such as: lizardite, hematite, dolomite, talc and magnesite (Table 1), occurs as lenses. It is poor in iron and nickel, but rich in magnesium and silica (Table 2).

General Composition of the Ržanovo Ore

Based on the studies of mineral associations as well as the major mineral phases or major nickel-bearing minerals in the deposit we can infer that the mineral association in the locality includes magnetite, hematite, clinocllore, talc, sepiolite, magnesioriebeckite, lizardite, dolomite, phlogopite, stilpnomelane, quartz, albite, pyrite, maghemite, pyrrhotite, digenite and millerite. Of the minerals mentioned above only five are constantly present, namely magnetite, hematite, clinocllore, talc and magnesioriebeckite.

According to the investigations carried out, and available data, the amount of the major minerals in the Ržanovo ore deposit is given in Table 4. The chemical compositions of the major mineral phases are shown in Tables 5–11.

Table 4. The average content (wt%) of the major minerals found in the Ržanovo deposit ores.

Mineral	Content
Amphibole	13.60
Clinocllore	10.65
Hematite	40.61
Magnetite	11.16
Talc	22.90
Total	98.92

Table 5. Magnetite (Mt), chromite (Chr), and hematite (Hm) chemical composition determined by EMP analysis (in wt %) and recalculations showing individual and total moles cation.

	Mt	Mt	Mt	Chr	Hm
Al ₂ O ₃			0.1	13.5	0.3
Cr ₂ O ₃	2.1	2.5	3.1	55.7	0.8
Fe ₂ O ₃	69.7	68.1	67.8	0.5	96.4
FeO	23.5	24.9	25.3	19.8	
MgO				8.9	0.2
MnO				0.5	
NiO	1.13	0.37	0.42	0.1	0.16
Total	96.43	95.87	96.72	99.00	97.86
	4(O) ^a	4(O)	4(O)	4(O)	3(O)
Al ³⁺			0.005	0.527	0.010
Cr ³⁺	0.065	0.078	0.096	1.458	0.017
Fe ³⁺	2.062	2.030	2.003	0.012	1.966
Fe ²⁺	0.773	0.825	0.831	0.548	
Mg ²⁺				0.439	0.008
Mn ²⁺				0.014	
Ni ²⁺	0.036	0.012	0.013	0.003	0.003
Total	2.936	2.945	2.948	3.001	2.004

^a The number of oxygen atoms taken for the moles cation calculations.

Table 6. Chemical composition of talc determined by EMP analysis (in mass %) and recalculations showing individual and total moles cation.

	Talc	Talc
Al ₂ O ₃	0.1	0.1
FeO	2.2	7.6
MgO	30.4	23.8
MnO	0.1	0.1
NiO	1.9	3.1
SiO ₂	60.6	60.8
Total	95.3	95.5
	11(O) ^a	11(O)
Al ³⁺	0.008	0.008
Fe ²⁺	0.119	0.421
Mg ²⁺	2.930	2.348
Mn ²⁺	0.005	0.006
Ni ²⁺	0.099	0.165
Si ⁴⁺	3.918	4.024
Total	7.079	6.972

^a The number of oxygen atoms taken for the moles cation calculations.

Table 7. Chemical composition of chlorite in the Ržanovo deposit ores determined by EMP analysis (in mass %) and recalculations showing individual and total moles cation.

	Chlorite	Chlorite	Chlorite	Chlorite
Al ₂ O ₃	17.0	14.57	16.4	15.7
Cr ₂ O ₃		4.65	2.75	3.28
FeO	14.1	16.86	13.7	17.7
K ₂ O		0.04	0.08	0.08
MgO	20.2	21.42	23.6	18.7
MnO	0.9	1.29		
Na ₂ O		0.03	0.80	0.80
NiO	7.7	1.15	2.55	4.07
SiO ₂	30.9	33.38	34.3	32.4
Total	90.80	93.39	94.18	92.73
	14(O) ^a	14(O)	14(O)	14(O)
Al ³⁺	1.993	1.645	1.800	1.809
Cr ³⁺		0.352	0.202	0.253
Fe ²⁺	1.173	1.351	1.067	1.447
K ⁺		0.005	0.010	0.010
Mg ²⁺	2.996	3.059	3.276	2.725
Mn ²⁺	0.076	0.105		
Na ⁺		0.006	0.144	0.152
Ni ²⁺	0.616	0.089	0.191	0.320
Si ⁴⁺	3.074	3.198	3.193	3.167
Total	9.928	9.810	9.883	9.883

^a The number of oxygen atoms taken for the moles cation calculations.

Chromite in the Ržanovo ore deposit belongs to the alumochromite group, with low nickel contents (about 0.1 %). Nickel-enriched magnetite surrounds chromite grains and occurs as idiomorphic forms with 0.3–1.3 % nickel. Some individual magnetite grains display a transition between chromite-ferrite-chromium-magnetite. These magnetite grains represent residues of parent rocks (i.e. serpentinites). They are depleted in nickel because the main nickel redistribution took place during metamorphism of the ores.

Hematite grains contain small amounts of nickel, most probably as the lattice was not sufficiently receptive for nickel or because hematite is mostly a secondary product.

Data shown in Table 6 indicate that talc is a nickeliferous phase, fairly rich in nickel (from 1.9 to

Table 8. Chemical composition of magnesioriebeckite (Amf) in the Ržanovo deposit ore determined by EMP analysis (in wt%) and recalculations showing individual and total moles cation.

	Amp	Amf	Amf
Al ₂ O ₃	0.9	0.9	0.93
CaO	0.3	2.3	1.44
FeO	19.36	20.14	17.90
K ₂ O			0.05
MgO	9.8	8.5	10.91
MnO	0.4	0.8	0.67
Na ₂ O	5.4	4.0	7.56
NiO	2.0	2.9	0.56
SiO ₂	54.3	53.3	56.51
Total	92.46	92.84	96.53
	23(O) ^a	23(O)	23(O)
Al ³⁺	0.164	0.166	0.162
Ca ²⁺	0.050	0.385	0.228
Fe ²⁺	2.508	2.634	2.210
K ⁺			0.009
Mg ²⁺	2.263	1.982	2.401
Mn ²⁺	0.052	0.106	0.084
Na ⁺	1.622	1.213	2.164
Ni ²⁺	0.249	0.365	0.067
Si ⁴⁺	8.410	8.336	8.341
Total	15.318	15.187	15.666

^a The number of oxygen atoms taken for the moles cation calculations.

3.1 %). Talc surrounding magnetite grains with chromite cores (analyses in Table 6) possesses an almost ideal structural formula in which magnesium in the octahedral position is replaced by ferrous iron and nickel. All this confirms our conclusions that it is a ferruginous talc which is transitional to minnesotaite.

Table 7 gives the composition of chlorites in the Ržanovo ore deposit determined by electron microprobe, which are rich in nickel and contain up to 7.7 %. Detailed microprobe and X-ray diffraction measurements determined that chlorite coincides with the nickeliferous clinocllore 2b type. The chromium content in some chlorites is also high, indicating them to be chromian chlorites.

Alkali amphiboles are represented by nickeliferous magnesioriebeckite, containing 0.56 to

Table 9. Chemical composition of stilpnomelane and biotite in the Ržanovo deposit ore determined by EMP analysis (in wt %) and recalculations showing individual and total moles cation.

	Stilpno-melane	Biotite
Al ₂ O ₃	5.9	11.12
CaO	0.1	
Cr ₂ O ₃	0.6	10.59
Fe ₂ O ₃	22.1	
FeO		13.63
K ₂ O	2.6	7.82
MgO	9.7	11.83
MnO	0.1	0.37
Na ₂ O	0.4	0.12
NiO	7.1	0.69
SiO ₂	47.1	39.52
TiO ₂		0.02
Total	95.70	95.71
	33(O) ^a	11(O)
Al ³⁺	1.503	0.985
Ca ²⁺	0.023	
Cr ³⁺	0.103	0.630
Fe ³⁺	3.594	
Fe ²⁺		0.857
K ⁺	0.717	0.750
Mg ²⁺	3.125	1.326
Mn ²⁺	0.018	0.024
Na ⁺	0.168	0.017
Ni ²⁺	1.234	0.042
Si ⁴⁺	10.179	2.972
TiO ₂		0.001
Total	20.664	7.604

^a The number of oxygen atoms taken for the moles cation calculations.

2.9 % NiO (Table 8). The sodium content in alkali amphiboles is variable depending on the conditions of metamorphic processes. Some amphiboles are closer to crossites and glaucophanes because of their higher sodium content.

From data shown in Table 9 we can infer that stilpnomelane is nickeliferous, and contains about 7 % NiO. Biotite is also slightly nickeliferous, contains relatively high chromium contents and is classified as a chromian biotite.

An important phenomenon noticed while determining the composition of the main ore

Table 10. Chemical composition of the matrix in the Ržanovo deposit ore determined by EMP analysis (in wt%).

	Massive magnetite ore	Schistose magnetite ore	Oolitic magnetite ore	Schistose hematite ore
Al ₂ O ₃	6.62	4.13	8.76	6.39
CaO	0.13	0.12	0.32	0.25
Cr ₂ O ₃	1.96	2.51	1.61	1.05
FeO	12.61	20.43	9.42	
Fe ₂ O ₃	31.16	50.49	23.27	24.31
K ₂ O	0.08		0.08	0.66
MgO	15.9	7.01	17.4	19.40
Na ₂ O	1.01	0.97	1.01	1.08
NiO	2.18	1.67	2.38	1.39
SiO ₂	29.6	15.2	36.6	43.40
TiO ₂	0.29	0.14	0.14	0.14
Total	101.54	102.67	100.99	98.07

Table 11. Chemical composition of sulphide minerals in the Ržanovo deposit ore determined by EMP analysis (in wt%).

	Millerite	Digenite	Bornite	Cobalt phase	Pyrite
Co	2.18			18.04	
Cu	0.38	77.67	64.59	41.94	
Fe	0.46	1.19	11.22	6.93	45.14
Ni	61.67	0.24		32.87	2.38
S	35.02	20.13	24.13		51.98
Total	99.71	99.23	99.94	99.78	99.5

minerals is the relatively large amount of fine-grained material in which it is very difficult to determine its mineral composition.

The composition of the fine-grained matrix was determined by the use of an electron microprobe and the results are given in Table 10.

A close look at the analyses in Table 10 shows that the sodium content in almost all samples is relatively high, indicating significant presence of alkali amphibole in the fine-grained matrix. Thus the matrix also contains a high nickel content.

Sulphide minerals are scarce and range from 1 % to 1.2 %. Sulphide minerals recognized include pyrite, pyrrhotine, millerite, digenite and bornite as well as cobalt sulphides. Their mineral compositions are given in Table 11.

Based on results of exploration, the following ore reserves are established and given in Table 12.

Table 12. Ore reserves (in thousands of tons) and the content of the elements (in wt %) in the Ržanovo ore deposit.

Categories of reserves	Amount of ore	Fe	Ni	Co	Cr
Proved	7.467	30.88	1.40	0.076	1.50
Probable	15.792	31.35	1.02	0.058	1.57
Possible	19.697	30.63	1.04	0.056	1.56
Total	42.956	30.94	1.036	0.060	1.55

Conditions for the Formation of the Ržanovo Ore Series Mineral Associations

The ore deposit belongs to the redeposited lateritic nickeliferous iron type formed by weathering of ultramafic rocks and additionally metamorphosed under greenschist facies conditions (Stojanov & Boev 1985).

Lateritization and formation of a typical lateritic crust of nontronite type took place during the Lower Cretaceous before the Albian. Erosion of nontronite crust and transportation of material to the sedimentary basin predated deposition of the Albian–Cenomanian limestones. Supply of material from primary lateritic crust was not continuous: there were periods when large amounts of non-lateritic material were introduced into the basin from surrounding source-rocks. Thus, some samples contain increased contents of trace elements which are not of an ultramafic origin. Because of this dilution of primary lateritic material, lower nickel contents characterize different parts of the ore-bearing sediments. During Albian–Cenomanian time, deposition of carbonate sediments and diagenesis of all redeposited material took place. Throughout these diagenetic and epigenetic processes alteration of primary minerals and formation of new minerals occurred (e.g., hematite, magnetite and chlorite as well as mixed layer

minerals formed instead of clay minerals). Some sulphides such as millerite and pyrite were also formed. The environment was rich in nickel which came from the weathering crust as nickel hydrocarbonates.

The Ržanovo ore series was affected by dynamometamorphism at the end of the Cretaceous and the Eocene or later (Stojanov & Boev 1985). The sedimentary products changed, under these processes into low-grade metamorphic rocks, producing the following mineral associations: magnetite, hematite, stilpnomelane, chlorite, talc, magnesioriebeckite, albite, calcite and dolomite. These minerals are not always found together. Certain associations can be found in various types of ferruginous rocks depending on the chemistry and activity of oxygen.

Based on this information it is inferred that formation temperatures of mineral associations were not typical of the greenschist facies (absence of epidote particularly indicates low temperature associations of about 250 °C or lower). The composition of albite and the ratio of ferrous iron and magnesium in chlorites also indicate low temperature associations (Maksimović & Panto 1982). The systems are also poor in aluminium. In systems rich in magnesium, calcium and silica, talc is formed at low temperatures and different pressures in a reaction between quartz and dolomite at a temperature of about 150 °C. However, the presence of riebeckite indicates that in some parts temperatures were higher (about 400 °C), or that magnesioriebeckite formed after a reaction of albite, chlorite and actinolite. All mineral associations are characterized by their high iron content and high to very high oxygen fugacity, or large hematite participation.

The occurrence of pyrite and millerite indicates local reducing conditions within the metamorphic system. Temperature increase resulted in the following mineral associations: smectite-chlorite-quartz, chlorite-talc-stilpnomelane-quartz, chlorite-actinolite-quartz and chlorite-magnesioriebeckite. This implies that in the Ržanovo area the mineral association was formed by epigenetic processes under low temperature greenschist facies conditions. The distribution of the mineral associations suggests

local temperature increase along the main tectonic lines as a result of pressure increase when the mineral associations of quartz-albite-muscovite-chlorite subfacies of green schists were formed. In some places, probably subjected to lower temperatures, mineral associations indicate lower temperature metamorphic conditions typical of the prehnite-pumpellyite facies.

Mineral Identification by Vibrational Spectroscopy

IR and Raman spectroscopy provide complementary information on the vibrational and bonding properties of the minerals. The bonding properties are reflected through the appearance of IR and Raman active vibrational bands at different wave numbers. Namely, depending on the structure and the present functional groups, the minerals show different spectral patterns which serve as individual fingerprints for each one. Therefore, vibrational (IR and Raman) spectroscopy is considered to be a powerful technique used to identify and characterize each mineral. In addition, the vibrational spectra can indicate evidence of mineral (im)purity.

The following minerals from the complex mineral paragenesis of the Fe-Ni Ržanovo deposit

were studied using IR and Raman spectroscopy: calcite, aragonite, dolomite (carbonates), hematite, 'magnetite', brucite (oxides and hydroxide), olivine, antigorite, chrysotile and talc (silicates). These minerals were selected for study because, crucially, only these minerals could be found as more or less well-formed crystal mineral types.

Calcite, CaCO_3 ; Aragonite, CaCO_3 and Dolomite, $\text{CaMg}(\text{CO}_3)_2$

The higher local symmetry of the CO_3^{2-} ions (D_3) in the structure of the studied rhombohedral carbonate minerals (calcite and dolomite) compared to the site symmetry of the same present anion in aragonite type (C_s) is manifested by the absence of ν_1 mode in their infrared spectra (Griffith 1969; Hellwege *et al.* 1970; White 1974; Paterson 1986; Jovanovski *et al.* 2002). Since ν_1 mode is IR active for C_s site symmetry of the CO_3^{2-} group, the band at 1083 cm^{-1} appears in the spectrum of aragonite (Figure 4a, Table 13). The absence of the corresponding band indicates an IR inactivity as seen in the spectra of the calcite and dolomite where CO_3^{2-} ions have D_3 symmetry (Figure 3b, c, respectively). Another striking method of easily discriminating between the aragonite and calcite (including dolomite) group is two-component

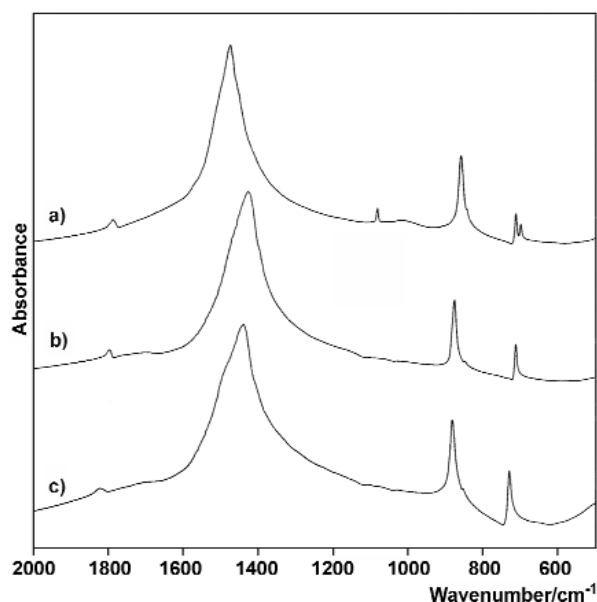


Figure 3. The IR spectra of studied carbonates from Ržanovo: aragonite (a), calcite (b), dolomite (c).

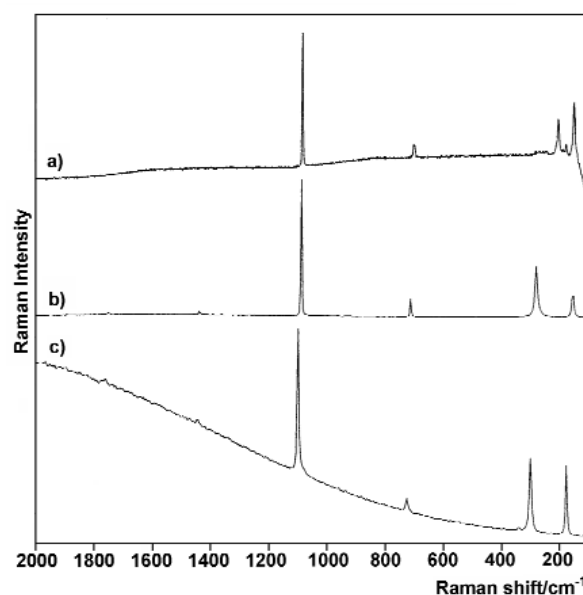


Figure 4. The Raman spectra of studied carbonates from Ržanovo: aragonite (a), calcite (b), dolomite (c).

Table 13. Vibrational frequencies for the studied carbonates (cm⁻¹).

Mode	IR			Raman		
	Aragonite	Calcite	Dolomite	Aragonite	Calcite	Dolomite
ν_1	1083 w ^a	–	–	1083 s	1086 s	1098 s
ν_2	858 m, 844 sh	876 m, 848 vw	880 m, 853 vw	–	–	–
ν_3	1474 s	1427 s	1439 s	–	1438 vw	1442 vw
ν_4	712 w, 699 vw	712 w	728 w	701 w	714 w	726 w
$\nu_1 + \nu_4$ ^b	1789 vw	1799 vw	1824 vw	–	1750 vw	1760 vw
A_g				205 m	282 m	302 m
B_{2g}				179 w		
B_{1g}				152 m	156 w	178 m

^a s – strong; m – medium; w – weak; sh – shoulder, v – very.

^b assignment given only for the Raman bands.

splitting of the ν_4 mode in the former mineral, giving rise to the bands at 712 and 699 cm⁻¹. In calcite and dolomite this mode appears as singlet at 712 and 728 cm⁻¹, respectively (Table 13). The remaining bands in the IR spectra of mentioned minerals are common and appear between 880 and 845 cm⁻¹ (two bands due to the ν_2 mode) and between 1824 and 1789 cm⁻¹.

It is evident that distinction between the rhombohedral carbonate minerals (calcite and dolomite type) using IR spectroscopy is more complex because they share the same structure. Their discrimination by IR spectroscopy is additionally complicated by the common appearance of these minerals in nature (Bermanec 1999). As discussed before, the D_3 symmetry of the CO_3^{2-} ions in their structures leads to the appearance of corresponding ν_2 , ν_3 and ν_4 modes at very similar frequencies. However, the discrepancy between both spectra is pronounced for the frequency of the band due to the ν_4 mode. It was shown that the frequency of the ν_4 mode is the most sensitive to the change of the divalent cation size [$r(\text{Ca}^{2+}) > r(\text{Fe}^{2+}) > r(\text{Mg}^{2+})$], being shifted to the higher frequencies [$\nu_4(\text{calcite}) < \nu_4(\text{siderite}) < \nu_4(\text{magnesite})$] for the smaller cations and smaller unit cell volume [$V(\text{calcite}) > V(\text{siderite}) > V(\text{magnesite})$] (Makreski & Jovanovski 2003). The smaller the cation is, the stronger the bending force constants are, causing closer stacking of the anions around it. The cationic radii of Ca^{2+} and average radii for Ca^{2+} and Mg^{2+} in calcite and dolomite are 1.00

and 0.86 Å, respectively (Shannon 1976), whereas the unit cell volume of calcite and dolomite are 367.85 and 320.24 Å³, respectively (Effenberger *et al.* 1981; Reeder 1983). Consequently, the frequency of the ν_4 mode in dolomite, $\text{CaMg}(\text{CO}_3)_2$, (728 cm⁻¹) follows this trend being observed at higher wavenumber than the corresponding mode in the calcite spectrum (712 cm⁻¹) (Table 13).

Raman spectra of the studied carbonates from Ržanovo are also used for mineral identification (Figure 4). Their band frequencies are listed in Table 13. As with the IR observations, the frequencies of the Raman ν_4 (and ν_1) active modes of the carbonates correlate well with the size of the corresponding cation radii. Thus, the frequency of the ν_4 mode almost linearly decreases with the increase of the cation radii in the series dolomite, calcite, aragonite [$r(\text{Ca}^{2+}, \text{Mg}^{2+})_{\text{av}} = 0.86$ Å, $\nu_4 = 726$ cm⁻¹; $r(\text{Ca}^{2+}) = 1.00$ Å, $\nu_4 = 714$ cm⁻¹; $r(\text{Ca}^{2+}) = 1.18$ Å, $\nu_4 = 701$ cm⁻¹]. A decreasing trend (but not linear) is also observed for the strongest band due to the ν_1 mode (1098, 1086 and 1083 cm⁻¹, respectively). The obtained results are in a good agreement with the corresponding Raman spectra (Griffith 1970; Herman *et al.* 1987; Kontoyannis & Vagenas 2000). The ν_2 mode is Raman inactive in all studied minerals, whereas two very weak bands arise at 1750 and 1760 cm⁻¹ ($\nu_1 + \nu_4$ combination) and at 1438 and 1442 cm⁻¹ (the ν_3 mode) in calcite and dolomite spectra, respectively (Figure 4, Table 13). The former band is inactive in

the Raman spectrum of aragonite (Tao *et al.* 1998) whereas the latter band is absent in the studied spectrum due to the higher noise-to-signal ratio.

In the lower Raman spectrum region (400–100 cm^{-1}) aragonite exhibits more peaks from the external optic modes than calcite and dolomite (Tao *et al.* 1998) (Figure 4). The preliminary assignment of the medium bands at 205, 282 and 302 cm^{-1} in aragonite, calcite and dolomite, respectively, is from A_g modes. The bands at 152 and 156 and 178 cm^{-1} in aragonite, calcite and dolomite spectrum could be assigned to the B_{1g} mode. The weak band at 179 cm^{-1} observed in the aragonite spectrum belongs to B_{2g} mode (Frech *et al.* 1980).

Hematite, Fe_2O_3 ; 'Magnetite', Fe_3O_4 v.s. Talc, $\text{Mg}_3\text{Si}_4\text{O}_{10}(\text{OH})_2$ and Brucite, $\text{Mg}(\text{OH})_2$

The IR spectrum of a mineral thought to be hematite is presented in the far IR region (Figure 5). The following activity for the normal modes are predicted on the basis of the factor group analysis $2A_{1g}(\text{R}) \oplus 3A_{2g} \oplus 5E_g(\text{R}) \oplus 2A_{1u} \oplus 2A_{2u}(\text{IR}) \oplus 4E_u(\text{IR})$ (McMillan & Hofmeister 1988). Although six IR bands were expected according to those observations, the number of bands registered in the literature varies (Table 14). Namely, the lowest and the highest frequency band are absent from the spectra discussed by Taylor *et al.* (1970) and by Farmer (1974), respectively, whereas both are absent in the spectrum obtained by McDevitt & Baun (1964). In spite of that, the studied IR spectrum of hematite reveals the expected six bands being in agreement with the corresponding results published by Serna *et al.* (1982).

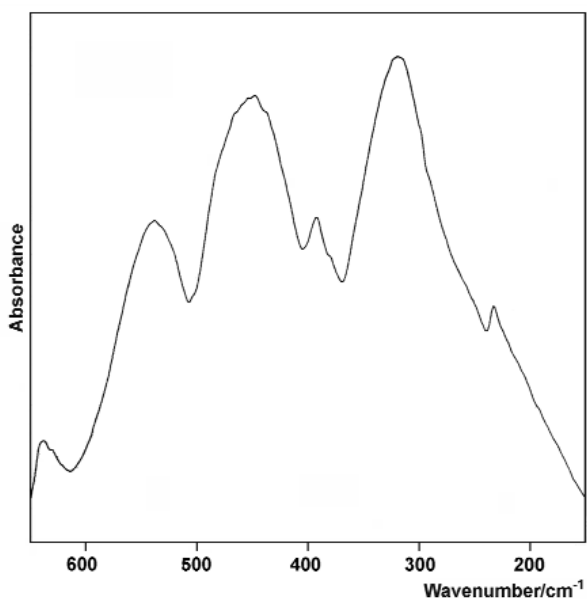


Figure 5. The far-IR spectrum of hematite from Ržanovo.

Where IR as well as Raman active modes have the same symmetry, the normal mode displacements associated with these vibrations are likely to be strongly mixed and it is difficult to discuss the detailed form of normal modes in the hematite structure (Blake *et al.* 1966). Exceptions are both IR active A_{2u} modes at 530 and 396 cm^{-1} where the oxygen motions, parallel and perpendicular to the plane of the four Fe atoms coordinating the oxygen, are involved. The remaining four bands at 643, 446, 307 and 233 cm^{-1} (Figure 5 and Table 14) have components of both Fe-O displacement with E_u symmetry (Makreski *et al.* 2004). Observed frequency shifts of the bands in the studied spectrum are due to the influence of particle shape and size (Serna *et al.* 1982).

Table 14. Band assignment in the IR spectra of hematite (in cm^{-1}).

Symmetry type	This work	Taylor <i>et al.</i> (1970)	Farmer (1974)	McDevitt & Baun (1964)	Serna <i>et al.</i> (1982)	
E_u^1	643 m ^a	625 sh	-	-	650 w	630 sh
A_{2u}^1	526 s	545 s	560 s	560 s	525 s	540 s
E_u^2	446 s	465 s	480 s	468 s	440 s	470 s
A_{2u}^2	397 w	370 sh	370 sh	370 sh	400 sh	380 w
E_u^3	307 s	335 s	345 s	325 s	-	335 s
E_u^4	233 w	-	235 w	-	229 w	229 w

^as – strong; m – medium; w – weak; sh – shoulder.

The Raman spectrum of the studied hematite sample (Figure 6a) exhibits all 7 Raman active modes predicted from the group analysis. Namely, both A_{1g} modes appear at 489 and 220 cm^{-1} , whereas the remaining five bands belonging to the E_g symmetry modes are observed at 603, 399, 295, 286 and 240 cm^{-1} (Table 15). The spectrum shows very pronounced agreement with the literature data for the corresponding mineral (Burgio & Clark 2001; Bouchard & Smith 2003; Villar & Edwards 2005). On the other hand, the appearance of two additional bands at 655 and 1297 cm^{-1} is mentioned only in the work of Bouchard & Smith (2003). The frequency of the former one coincides with 660 cm^{-1} band, typical for magnetite Raman spectra (Figure 6b) and according to these authors, its origin is connected with the possible partial transformation of hematite into magnetite under the laser beam. The latter band (1297 cm^{-1}) corresponds to a 'two magnon-effect' that involves an indirect electric-dipole coupling which proceeds through a spin-orbit interaction (Bouchard & Smith 2003) (Table 15). The band of the same origin is evidently present in the Raman

spectrum of magnetite from Damjan registered around 1300 cm^{-1} (Figure 6b).

Magnetite crystals from Ržanovo occur as small euhedral octahedra on the talc rich specimens. Therefore, the magnetite crystals were carefully picked up from the talc specimen under microscope and then powdered. Surprisingly, the recorded IR spectrum did not show similarities with the previously recorded magnetite sample from Damjan (Figure 7a and 7b). Furthermore, strong absorption band observed around 1020 cm^{-1} , associated with the shoulder on the higher frequency side, was taken as a strong indication that the studied mineral contains significant amount of some silicate impurity or represents the silicate mineral type itself. Since the crystals contemplated as magnetite were picked up from the talc basis specimen, the spectrum was compared with the IR spectrum of talc (Figure 7c). It was shown that the spectra present great resemblance between each other (Table 16). The result served as an assumption that the studied crystals were, in fact, talc, although magnetite is only present on their surface (matrix cemented by talc),

Table 15. Band assignment in the Raman spectra of hematite (in cm^{-1}).

This work	Villar & Edwards 2005	Burgio & Clark 2001	Bouchard & Smith 2003	Symmetry type
1297 s ^{a,b}			1330 s	
655 w			660 w	
603 m	611 m	609 w	611 m	E_g
-	561 w	-	-	
-	502 w	-	-	
489 w	492 w	495 w	498 w	A_{1g}
399 s	409 m	408 m	411 m	E_g
295 s, sh	292 s	299 s, sh	299 s, sh	E_g
286 s	-	290 s	291 s	E_g
240 w	244 vw	243 w	245 vw	E_g
220 m	224 m	224 s	224 w	A_{1g}

^a s- strong; m- medium; w- weak; sh- shoulder, v- very.

^b band corresponds to so called 'two magnon-effect'.

^c According to Bouchard & Smith (2003) as a result of possible partial transformation of hematite into magnetite under the laser beam.

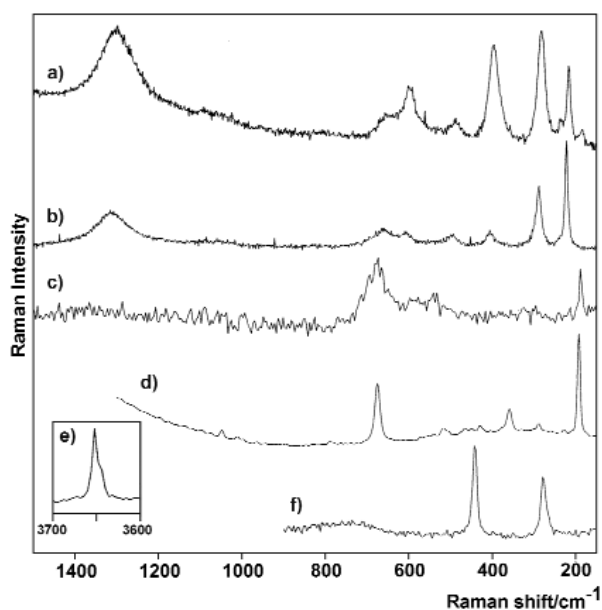


Figure 6. The Raman spectra of hematite (a), talc ('magnetite') (c), talc (d) and brucite (f) from Ržanovo. The Raman spectrum of magnetite from Damjan (b) is shown for comparison. The OH stretching region of brucite is separately presented (e).

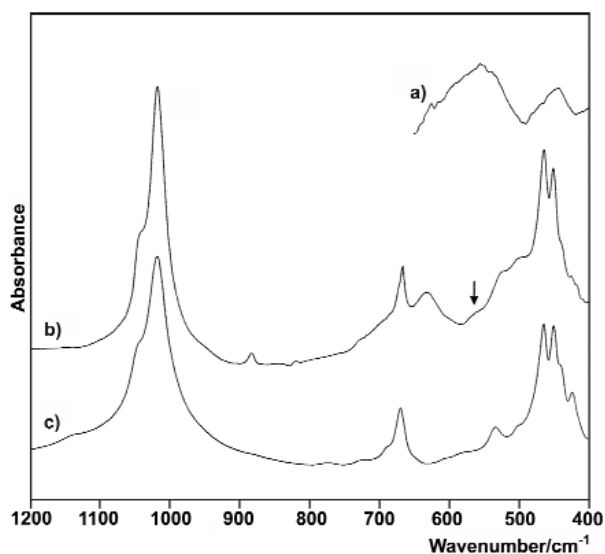


Figure 7. The IR spectra of magnetite (a) from Damjan, talc ('magnetite') (b) and talc (c) from Ržanovo. The arrow refers to the shoulder which corresponds to the frequency of the strongest band in the IR spectrum of magnetite (a).

being hardly recognizable from the IR spectrum of the studied sample except the appearance of the shoulder around 560 cm^{-1} (Figure 7b).

In general, the results of the Raman spectroscopy study confirmed the supposition that the studied mineral represents the talc sample (Figure 6c, d). Thus, despite the high noise-to-signal ratio (Figure 6c), the studied spectrum is different from its magnetite counterpart (Figure 6b) whereas the great similarity with the talc Raman spectrum is clearly expressed (Figure 6d). In spite of that, the broadening of the band around 675 cm^{-1} could be eventually related to the presence of a very small content of magnetite in the studied sample. A systematic study of the IR and Raman spectra of talc, as a part of the sheet silicate series from Macedonia, was recently carried out (Šontevska *et al.* 2006). Therefore, we present here only the proposed band assignments without further discussion on their origin (Tables 16 & 17, first columns).

According to the factor group analysis there are six (three IR and three Raman active) allowed lattice mode indicated for brucite. In addition, there are IR and Raman active internal modes (Mitra 1962). The studied IR spectrum of brucite (Figure 8) is characterized by the appearance of two strong bands around 3700 and 440 cm^{-1} followed by several weak and very weak bands or shoulders in between (Table 18).

Table 16. The IR assignment for the identified silicate minerals from the Ržanovo deposit.

Talc	Assignment	Chrysotile	Assignment	Antigorite	Assignment	Forsterite	Assignment
3677 m ^a	$\nu(\text{OH})$	3688 s	$\nu(\text{OH})$	3699 sh ^a	$\nu(\text{OH})$	1000 sh	$\nu_3(\text{Si-O-Si})$
3661 w	$\nu(\text{OH})$	3646 w	$\nu(\text{OH})$	3678 s	$\nu(\text{OH})$	982 vs	$\nu_3(\text{Si-O-Si})$
3644 vw	$\nu(\text{OH})$	1078 s	$\nu(\text{Si-O}_{\text{nb}}\text{-Si})$	1083 s	$\nu(\text{Si-O}_{\text{nb}}\text{-Si})$	955 w	-
1047 sh	$\nu_3(\text{Si-O}_{\text{nb}}\text{-Si})$	1022 sh	$\nu(\text{Si-O}_{\text{nb}}\text{-Si})$	987 vs	$\nu(\text{Si-O}_b\text{-Si})$	915 sh	-
1018 vs	$\nu_1(\text{Si-O}_{\text{nb}}\text{-Si})$	961 vs	$\nu(\text{Si-O}_b\text{-Si})$	958 sh	$\nu(\text{Si-O}_b\text{-Si})$	886 vs	$\nu_3(\text{Si-O-Si})$
774 vw	-	611 s	$\delta(\text{OH})$	758 vw	-	839 w	$\nu_1(\text{Si-O-Si})$
728 vw	-	556 vw	$\delta(\text{Si-O-Si})$	639	sh $\delta(\text{OH})$	608 s	$\nu_4(\text{Si-O-Si})$
669 s	L(OH)	455 sh	-	618 m	$\delta(\text{OH})$	577 vw	-
533 m	$\nu(\text{Mg-OH})$	438 vs	$\delta(\text{Si-O-Si})$	564 m	$\delta(\text{Si-O-Si})$	547 sh	-
465 vs	T(OH)	405 w	-	506 vw	-	522 sh	-
450 vs	$\delta(\text{Si-O-Si})$			445 vs	$\delta(\text{Si-O-Si})$	505 vs	$\nu_4(\text{Si-O-Si})$
439 sh	-			434 sh	-	470 w	-
424 m	-			400 w	-	417 vs	$\nu_2(\text{Si-O-Si})$
						401 sh	-
						379 vw	-

^a s- strong; m- medium; w- weak; sh- shoulder, v- very.

Table 17. The Raman data for the studied silicates from the Ržanovo deposit.

Talc	Assignment	Chrysotile	Assignment	Antigorite	Assignment	Forsterite	Assignment
1048 w ^a	$\nu(\text{Si-O}_{\text{nb}}-\text{Si})$	1106 m	$\nu_{\text{as}}(\text{Si-O}_{\text{nb}}-\text{Si})$	1099 w	$\nu_{\text{as}}(\text{Si-O-Si})$	960 w	$\nu_3(\text{Si-O-Si})$
675 s	$\nu(\text{Si-O-Si})$	944 s	–	1090 w	$\nu_{\text{as}}(\text{Si-O-Si})$	919 sh	–
517 w	$\delta(\text{Si-O-Si})$	692 vs	$\nu(\text{Si-O-Si})$	1048 w	$\nu_{\text{as}}(\text{Si-O-Si})$	876 sh	–
430 w	$\nu(\text{Mg-O})$	626 m	$\nu(\text{Mg-OH})$	682 m	$\nu_{\text{s}}(\text{Si-O-Si})$	855 vs	$\nu_3(\text{Si-O-Si})$
361 m	$\delta(\text{Si-O-Si})$	392 vs	$\delta(\text{Si-O-Si})$	628 w	$\nu(\text{Mg-OH})$	823 vs	$\nu_1(\text{Si-O-Si})$
289 m	$\nu(\text{Mg-O})$	348 m	$\delta(\text{Si-O-Si})$	372 m	$\delta(\text{Si-O-Si})$	605 vw	$\nu_4(\text{Si-O-Si})$
228 w	$\nu(\text{Mg-O})$	320 w	$\delta(\text{Si-O-Si})$	230 m	$\text{O}_{\text{nb}}\cdots\text{H-O}$	588 w	–
193 vs	Ext. mode	306 w	$\delta(\text{Si-O-Si})$	224 m	Ext. mode	542 w	$\nu_4(\text{Si-O-Si})$
114 m	Ext. mode	235 s	$\text{O}_{\text{nb}}\cdots\text{H-O}$	116 s	Ext. mode	430 w	$\nu_4(\text{Si-O-Si})$
		206 w	$\nu(\text{Mg-O})$			369 vw	$\nu_2(\text{Si-O-Si})$
		132 s	Ext. mode			336 vw	–
		118 m	Ext. mode			326 vw	$\nu_2(\text{Si-O-Si})$
						302 vw	–
						223 vw	–

^as – strong; m – medium; w – weak; sh – shoulder, v – very.

Table 18. Band assignment in the IR spectra of brucite (in cm^{-1}).

This work	Frost & Klopogge 1999	Nicodom 1998	Ryskin 1974	Assignment
3698 s ^a	3698	3695 vs	3698	Brucite, O–H stretch
3271 vw	3275	3275 w	–	Brucite, Strongly bonded water
1628 vw	1630	1605 w	–	Brucite, H ₂ O bending
1076 vw	1080	–	–	Serpentine impurity, Si–O stretch
1049 vw	1045	–	–	Talc impurity, Si–O stretch
1014 vw	1017	–	–	Talc impurity, Si–O stretch
954 vw	960	–	–	Serpentine impurity, Si–O stretch
568 m	560	565 m	–	Brucite, MgO translation mode
441 vs	440	445 s	415	Brucite, MgO translation mode

^as – strong; m – medium; w – weak; sh – shoulder, v – very.

The IR band at 3698 cm^{-1} clearly arises from the hydroxyl stretching vibration, whereas the underlying scarcely recognizable band in this region, found at 3271 cm^{-1} (Frost & Klopogge 1999) should be attributed to the strongly bonded water vibration. Here, the positions of the remaining IR bands are generally in agreement with previously recorded data (Frost & Klopogge 1999), but it is apparent that, despite the simple chemical formula of the studied mineral, there are considerable differences between the absorption spectra of the other two natural

brucite samples (Ryskin 1974; Nicodom 1998) (Table 18). This is explained by the difficulty in collecting pure naturally occurring brucite crystals because of frequent contamination by other minerals such as carbonates (dolomite, calcite, magnesite) and especially sheet silicates like talc and serpentine with which it shares a layered structure (Nesse 2000). Therefore, the very weak bands at 1076, 954 and $1049, 1014 \text{ cm}^{-1}$ probably result from very small amounts of serpentine and talc impurities, since the mentioned frequencies coincide very well with the

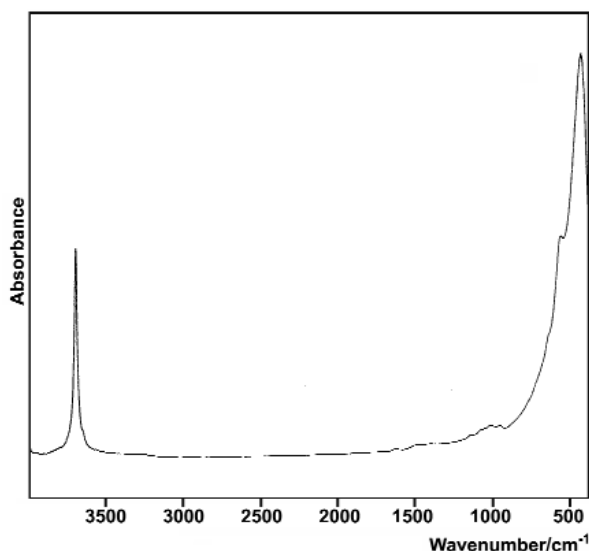


Figure 8. The IR spectrum of brucite from Ržanovo.

strongest IR bands for those minerals collected from the same locality (Šontevska *et al.* 2006). The lower frequency bands at 568 and 441 cm^{-1} are attributed to Mg–O translational modes (Table 18).

The Raman spectrum of the mineral thought to be brucite is presented in Figure 6e and 6f, and the band assignments are presented in Table 19. The highest wavenumber band at 3652 cm^{-1} is attributed to the symmetric internal O–H stretching vibration (with A_{1g} symmetry) and is in agreement with the literature (Dawson *et al.* 1973; Duffy *et al.* 1995; Weckler & Lutz 1996) whereas the shoulder at the lower wavenumber side at 3646 cm^{-1} is registered only by Duffy *et al.* (1995). The lattice vibrations in the Raman spectrum of brucite consist of translational modes that are parallel and perpendicular to the c -axis as well as the rotational vibrations of the OH ions. The former ones with A_{1g} and E_g symmetry give rise to the bands at 444 cm^{-1} (strong) and 280 cm^{-1} (strong). The third one (again with E_g symmetry), expected around 730 cm^{-1} (Dawson *et al.* 1973; Duffy *et al.* 1995), is broad and barely recognizable due to the expressed signal to noise ratio in this region (Figure 6f). However, the band wavenumbers and intensities are in very good agreement with the previous published data for this mineral type (Table 19), confirming that the mineral is brucite.

Table 19. Band assignment in the Raman spectra of brucite (in cm^{-1}).

This work	Duffy <i>et al.</i> 1995	Dawson <i>et al.</i> 1973	Assignment (symmetry mode)
3652 s	3661 s	3652	$\nu(\text{OH}), A_{1g}$
3646 sh	3652 s	–	$\nu(\text{OH}), A_{1g}$
728 w	727 w	725	$\text{R}(\text{M–O}), E_g$
444 s	445 s	443	$\text{T}(\text{M–O}), A_{1g}$
280 s	280 s	280	$\text{T}(\text{M–O}), E_g$

^as– strong; m– medium; w– weak; sh– shoulder, v– very.

Chrysotile, $(\text{Mg}, \text{Fe}^{2+})_3\text{Si}_2\text{O}_5(\text{OH})_4$; Antigorite, $(\text{Mg}, \text{Fe}^{2+})_3\text{Si}_2\text{O}_5(\text{OH})_4$ and Olivine var. Forsterite, Mg_2SiO_4

Serpentine mineralization in Ržanovo locality is represented by two minerals: chrysotile and antigorite. An attempt to identify these minerals was made using vibrational (IR and Raman) spectroscopy although similarity due to their isomorphism was expected.

The first discrimination feature between their IR spectra is the stretching OH region (3800–3600 cm^{-1}), where the corresponding bands from the two crystallographically different O–H bonds are much better resolved in the case of chrysotile (Figure 9a, b).

The similarity between the spectra is more evident in the SiO_4 region (Figure 9c, d; Table 16). In spite of that, the analytical bands in this region (e.g., the bands that appear only in the spectrum of one of both minerals and differentiate between each other) are found at 1022 cm^{-1} (chrysotile) and 758, 639, 506, 434 cm^{-1} (antigorite).

The Raman spectra of chrysotile and antigorite (the latter shows highly expressed noise-to-signal ratio and is of somewhat lower quality) are presented in Figure 10a and 10b. Without detailed assignment of the bands made in our previous work (Šontevska *et al.* 2006), it could be concluded that the trend of band frequency decrease is characteristic for the antigorite spectrum (Figure 10).

The isomorphous forsterite (Mg_2SiO_4) and fayalite (Fe_2SiO_4) are the end-members of the olivine [$(\text{Mg}, \text{Fe})_2\text{SiO}_4$] solid solution. In order to identify the

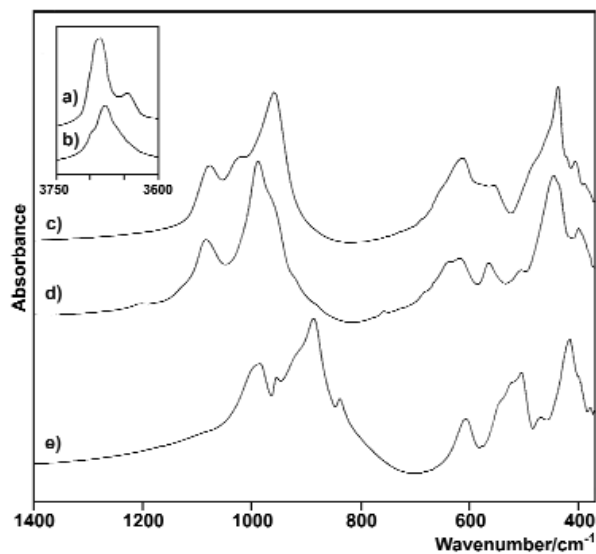


Figure 9. The IR spectra of chrysotile (a, c), antigorite (b, d) and olivine var. forsterite (e) from Ržanovo.

studied mineral, its IR and Raman spectra were recorded (Figures 9e & 10c, respectively; Tables 16 & 17).

In our recent work, it was found that the IR bands in the olivines show a frequency shift to lower values with iron content increasing especially for the bands above 600 cm^{-1} (Makreski *et al.* 2005). This criterion applied to our studied specimen led to conclusion that it is rather forsterite, Mg_2SiO_4 instead of being fayalite, Fe_2SiO_4 .

The Raman spectrum of olivine (Figure 10c) confirmed that the strongest peaks at 855 and 823 cm^{-1} due to the $\nu_3(\text{Si-O-Si})$ and $\nu_1(\text{Si-O-Si})$ vibrations, respectively as well as the weak band at 919 and 960 cm^{-1} [$\nu_3(\text{Si-O-Si})$] coincide with previously recorded bands of forsterite (Griffith 1969; Guyot *et al.* 1986) (Table 17). The similarities between our and previous literature data for the lower frequency peaks (where the bending modes appear) are also well expressed in the region below 800 cm^{-1} .

Conclusions

The Ržanovo Fe-Ni deposit is one of the largest deposits of nickelous iron in South Eastern Europe.

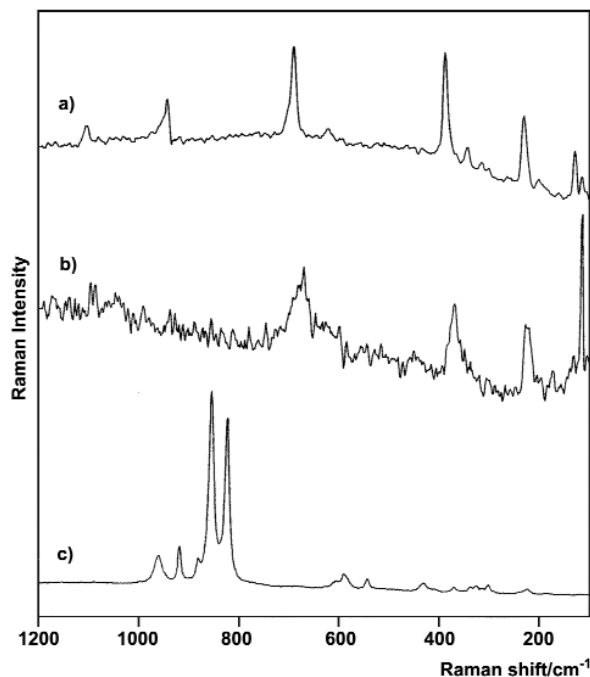


Figure 10. The Raman spectra of chrysotile (a), antigorite (b) and olivine var. forsterite (c) from Ržanovo.

Geotectonically situated in the west ophiolitic belt of the Vardar zone, it represents precipitated lateritic crust that later, in the young Alpien orogenic phase, was subjected to greenschist facies dynamothermal metamorphism. Several structural/textural types of ore have been found and described, such as massive magnetite ore, schistose magnetite ore, oolitic magnetite ore, schistose hematite ore, compact hematite ore, riebeckite schists, stilpnomelane schists, dolomite-talc schists, talc schists and serpentinites. The main mineral phases are found to be magnetite, hematite, talc, clinocllore and amphibole, with smaller proportions of stilpnomelane, dolomite, sepiolite, lizardite, various sulphide minerals and others. Most of the nickel present in the Ržanovo deposit is in silicate minerals.

Furthermore, the investigations carried out on the minerals of the Ržanovo deposit indicated that IR and Raman spectroscopy can be used as a tool to determine the collected minerals hematite, brucite, calcite, aragonite, dolomite, talc, antigorite, chrysotile and olivine. Also, the mentioned techniques enable a rapid check on the purity of the minerals that very often give an unequivocal

opportunity for their identification, especially as the mineral identification should not be based on the morphological features alone. As a consequence, sometimes, the characterization is misleading, as with the morphologically identified crystals of magnetite that is, in fact, coated talc (magnetite is only present on their surface). Also, both vibrational techniques are sensitive to mineral impurities and whenever possible both should be used together for mineral identification and characterization.

References

- BERMANEC, V. 1999. *Sistematska Mineralogija – Mineralogija Nesilikata [Systematic Mineralogy – Mineralogy of the Nesilicates]*. Targa Publisher, Zagreb [in Croatian].
- BLAKE, R.L., HESSEVICK, R.E., ZOLTAI, T. & FINGER, L.W. 1966. Refinement of the hematite structure. *American Mineralogist* **51**, 123–129.
- BOEV, B. & JANKOVIC, S. 1996. Nickel and nickeliferous iron deposits of the Vardar zone (SE Europe) with particular reference to the Ržanovo-Studena Voda ore bearing series. *Special Issue of the Stip Faculty of Mining and Geology* **3**, 270–278.
- BOEV, B., MIRCOVSKI, V. & KORIKOVSKI, S. 1999. Rodingite rocks in the Jurassic serpentinite masses in the area of Ržanovo, Republic of Macedonia. *Geologica Macedonica* **13**, 75–84.
- BOUCHARD, M. & SMITH, D.C. 2003. Catalogue of 45 reference Raman spectra of minerals concerning research in art history or archaeology, especially on corroded metals and coloured glass. *Spectrochimica Acta Part A* **59**, 2247–2266.
- BURGIO, L. & CLARK, R.J.H. 2001. Library of FT-Raman spectra of pigments, minerals, pigment media and varnishes, and supplement to existing library of Raman spectra of pigments with visible excitation. *Spectrochimica Acta Part A* **57**, 1491–1521.
- DAWSON, P., HADFIELD, E.D. & WILKINSON, G.R. 1973. The polarized infra-red and Raman spectra of Mg(OH), and Ca(OH). *Journal of Physics and Chemistry of Solids* **34**, 1217–1225.
- DUFFY, T.S., MEADE, C., FEI, Y., MAO, HO-K. & HEMLEY, R.J. 1995. High-pressure phase transition in brucite, Mg(OH)₂. *American Mineralogist* **80**, 222–230.
- EFFENBERGER, H., MEREITER, K. & ZEMANN, J. 1981. Crystal structure refinements of magnesite, calcite, rhodochrosite, siderite, smithsonite and dolomite with discussion of some aspects of the stereochemistry of calcite type carbonates. *Zeitschrift fuer Kristallographie* **156**, 233–243.
- FARMER, V.C. 1974. The anhydrous oxide minerals. In: FARMER, V.C. (ed), *The Infrared Spectra of Minerals*. Mineralogical Society, London, 183–204.
- FRECH, R., WANG, E.C. & BATES, J.B. 1980. The I.R. and Raman Spectra of CaCO₃ (aragonite). *Spectrochimica Acta Part A* **36**, 915–919.
- FROST, R.L. & KLOPPROGGE, J.T. 1999. Infrared emission spectroscopic study of brucite. *Spectrochimica Acta Part A* **55**, 2195–2205.
- GUYOT, F., BOYER, H., MADON, M., VELDE, B. & POIRIER, J.P. 1986. Comparison of the Raman microprobe spectra of (Mg,Fe)₂SiO₄ and Mg₂GeO₄ with olivine and spinel structures. *Physics and Chemistry of Minerals* **13**, 91–95.
- GRAFENAUER, S. & STRMOLE, D. 1966. Zlog in mineralna sestava nikljenosnih železovih rud Ržanova [Mineral composition of the nickel-iron ores in Ržanovo]. In: *Proceedings of the Stip Faculty of Mineralogy and Metallurgy* **1**, 51–62 [in Slovenian with English abstract].
- GRIFFITH, W.P. 1969. Raman spectroscopy of minerals. *Nature* **224**, 264–266.
- GRIFFITH, W.P. 1970. Raman studies on rock forming minerals. Part II. Minerals containing MO₃, MO₄, and MO₆ groups. *Journal of Chemical Society A* **1**, 286–291.
- HELLWEGE, K.H., LESCH, W., PLIHAL, M. & SCHAACK, G. 1970. Zwei-phononen-absorptionsspektren und dispersion der schwingungszweige in kristallen der kalkspatstruktur [Two phonon absorption spectra and dispersion branches of oscillation in crystals of the calcspat structure]. *Zeitschrift fuer Physik* **232**, 61–86 [in German with English Abstract].
- HERMAN, R.G., BOGDAN, C.E., SOMMER A.J. & SIMPSON, D.R. 1987. Discrimination among carbonate minerals by Raman spectroscopy using the laser microprobe. *Applied Spectroscopy* **41**, 437–440.
- NICODOM 1998. *Inorganic Library of FT IR Spectra – Minerals*, Nicodomo Ltd., Prahás.
- IVANOV, T. 1959. Niklonosno gvozdje kod Ržanova na Kožufu (N.R. Makedonija) [Nickelous iron near to Ržanovo on the Kožuf (P.R. Macedonia)]. In: *Proceedings of the IIIth Congress of Geologists from Yugoslavia*, 249–264 [in Serbian with English abstract].
- IVANOV, T., MISAR, Z., BOWES, D.R., DUDEK, A., DUMURGANOV, N., JAROS, J. & JELINEK, E. 1987. The Demir Kapija-Gevgelija ophiolite massiv, Macedonia. *Ofioliti* **12**, 457–478.

Acknowledgments

Financial support from the Ministry of Education and Science of the Republic of Macedonia is gratefully acknowledged. The authors cordially thank Prof. Mile Petkovski from ESRA University, Skopje, for technical editing of Figure 2. English of the final text is edited by John A. Winchester.

- JOVANOVSKI, G., STEFOV, V., ŠOPTRAJANOV, B. & BOEV, B. 2002. Minerals from Macedonia. IV. Discrimination between some carbonate minerals by FTIR spectroscopy. *Neues Jahrbuch Mineralogie, Abhandlungen* **177**, 241–253.
- KARAMATA, S. 2006. Review of ophiolite belts in the northern part of the Balkan Peninsula. In: *Proceedings of the Mesozoic Ophiolite Belt of the Northern Part of the Balkan Peninsula, Belgrade-Banja Luka*, 59–61.
- KONTOYANNIS, C.G. & VAGENAS, N.V. 2000. Calcium carbonate phase analysis using XRD and FT-Raman spectroscopy. *Analyst* **125**, 251–255.
- MAKRESKI, P. & JOVANOVSKI, G. 2003. Minerals from Macedonia. IX. Distinction between some rhombohedral carbonates by FTIR spectroscopy. *Bulletin of the Chemists and Technologists of Macedonia* **22**, 25–32.
- MAKRESKI, P., JOVANOVSKI, G., KAITNER, B., STAFILOV, T., BOEV, B. & CIBREV, D. 2004. Minerals from Macedonia. X. Separation and identification of some oxide minerals by FT IR spectroscopy, AAS, EAS-ICP and powder XRD. *Neues Jahrbuch Mineralogie, Abhandlungen* **180**, 215–243.
- MAKRESKI, P., JOVANOVSKI, G. & STOJANČESKA, S. 2005. Minerals from Macedonia. XIII. Vibrational spectra of some commonly appearing nesosilicate minerals. *Journal of Molecular Structure* **744–747**, 79–92.
- MAKSIMOVIĆ, Z. & PANTO, GY. 1981. Nickel-bearing phlogopite from the nickel-iron deposit Studena Voda (Macedonia). *Bulletin of the Serbian Academy of Sciences* **80**, 1–6.
- MAKSIMOVIĆ, Z. & PANTO, GY. 1982. The main nickel bearing phases in the Ržanovo deposit, Yugoslavia; chlorite, talc, stilpnomelane and magnesioriebeckite. *Bulletin of the Serbian Academy of Sciences* **72**, 77–96.
- MCDEVITT, N.T. & BAUN, W.L. 1964. Infrared absorption study of metal oxides in the low frequency region (700–240 cm^{-1}). *Spectrochimica Acta* **20**, 799–808.
- MCMILLAN, P.F. & HOFMEISTER, A.M. 1988. Infrared and Raman spectroscopy. In: HAWTHORNE, F.C. (ed), *Spectroscopic Methods in Mineralogy and Geology*. Reviews in Mineralogy and Geochemistry **18**, 99–157.
- MITRA, S.S. 1962. Vibration spectra of solids. In: SEITZ, F. & TURNBULL, D. (eds), *Solid State Physics*. Academic Press, New York, 1–80.
- NESSE, W.D. 2000. *Introduction to Mineralogy*. Oxford University Press, New York.
- PATERSON, W.G. 1986. Identifying minerals from their infra-red spectra. *School Science Reviews* **68**, 253–264.
- REEDER, R.J. 1983. Crystal chemistry of the rhombohedral carbonates. *Reviews in Mineralogy and Geochemistry* **11**, 1–47.
- RYSKIN, YA.I. 1974. The vibrations of protons in minerals hydroxyl, water and ammonium. In: FARMER, V.C. (ed), *The Infrared Spectra of Minerals*. Mineralogical Society, London, 137–182.
- SERNA, C.J., RENDON, J.L. & IGLESIAS, J.E. 1982. Infrared surface modes in corundum-type microcrystalline oxides. *Spectrochimica Acta Part A* **38**, 797–802.
- SHANNON, R.D. 1976. Revised effective ionic radii and systematic studies of international distances in halides and chalcogenides. *Acta Crystallographica Part A* **32**, 751–754.
- STOJANOV, R. & BOEV, B. 1985. Metamorphism of Ni-Fe ores from Ržanovo-Studena Voda and the zone Almopias. *Geologica Macedonica* **1**, 195–201.
- ŠONTEVSKA, V., JOVANOVSKI, G. & MAKRESKI, P. 2006. Minerals from Macedonia. XIX. Vibrational spectra of some sheet silicate minerals. *Journal of Molecular Structure* **834–836**, 318–327.
- TAO, J., XU, Y., XU, Z., WU, J. & XU, D. 1998. FT-Raman and FT-IR study on calcite and antigorite. In: HEYNS, P.M. (ed), *Proceedings of the XVIIth International Conference of Raman Spectroscopy*, Wiley, 716–717.
- TAYLOR, D.G., NENADIC, C.M. & CRABLE, J.V. 1970. Infrared spectra for mineral identification. *American Industrial Hygiene Association Journal* **31**, 100–108.
- VILLAR, S.E.J. & EDWARDS, H.G.M. 2005. Near-infrared Raman spectra of terrestrial minerals relevance for the remote analysis of Martian spectral signatures. *Vibrational Spectroscopy* **39**, 88–94.
- WECKLER, B. & LUTZ, H.D. 1996. Lattice vibration spectra, Part LXXXIX, Near-infrared spectra of $M(\text{OH})\text{Cl}$ ($M = \text{Ca}, \text{Cd}, \text{Sr}$), $\text{Zn}(\text{OH})\text{F}$, $\gamma\text{-Cd}(\text{OH})_2$, $\text{Sr}(\text{OH})_2$, and brucite-type hydroxides $M(\text{OH})_2$ ($M = \text{Mg}, \text{Ca}, \text{Mn}, \text{Fe}, \text{Co}, \text{Ni}, \text{Cd}$). *Spectrochimica Acta Part A* **52**, 1507–1513.
- WHITE, W.B. 1974. The carbonate minerals. In: FARMER, V.C. (ed), *The Infrared Spectra of Minerals*. Mineralogical Society, London, 227–284.